Strojniški vestnik - Journal of Mechanical Engineering 64(2018)1, 26-36

DOI:10.5545/sv-jme.2017.4989 Original Scientific Paper
Received for review: 2017-10-14
Received revised form: 2017-11-27
Accepted for publication: 2017-11-29

Numerical Study of Heat Transfer Enhancement for Low-Pressure Flows in a Square Cavity with Two Fins Attached to the Hot Wall Using Al_2O_3-Air Nanofluid

Wael Al-Kouz[1,*] – Suhil Kiwan[2] – Ammar Alkhalidi[3] – Ma'en Sari[4] – Aiman Alshare[1]

[1] German Jordanian University, Mechatronics Engineering Department, Jordan
[2] Jordan University of Science and Technology, Mechanical Engineering Department, Jordan
[3] German Jordanian University, Energy Engineering Department, Jordan
[4] German Jordanian University, Mechanical and Maintenance Engineering Department, Jordan

The gaseous low-pressure nanofluid flow of a steady-state two-dimensional laminar natural convection heat transfer in a square cavity of length L with two attached solid fins to the hot wall is numerically investigated. Such flows are found in many engineering applications, such as nuclear reactors and electronic cooling equipment. Physical parameter ranges in this study are as follows: $0 \le Kn \le 0.1$, $10^3 \le Ra \le 10^6$, $0 \le \phi \le 0.2$, L_F/L takes the value of 0.5, H_F takes the values of 0.25 to 0.75. Simulation results show that Nusselt number depends directly on the Rayleigh number and inversely on the Knudsen number. In addition, it is found that heat transfer will be enhanced by dispersing the nanoparticles of Al_2O_3 in the base low-pressure gaseous flow. Moreover, it is found that the Nusselt number of such flows increases as the nano-particle volume fraction increases for the investigated range of volume fractions considered in this study. In addition, a correlation of the Nusselt number among all the investigated parameters in this study is proposed as $Nu = 0.2196\, Ra^{0.0829}\, Kn^{-0.511}\, \phi^{0.104}$.

Keywords: natural convection, heat transfer, low pressure, cavity

Highlights

- *This research aims to study numerically laminar steady natural convection flow in a cavity in which two solid fins are attached to the hot side wall.*
- *The cavity was filled with air-Al_2O_3 nanofluid.*
- *The effects of the Knudsen number, the Rayleigh number and the volume fraction of the nanoparticles were investigated.*
- *It was found that the heat transfer rate is enhanced by increasing the volume fraction of the nanoparticles, increasing the Rayleigh number and decreasing the Knudsen number.*

0 INTRODUCTION

Natural convection in enclosed cavities can be found in many engineering applications, such as those found in nuclear reactor cooling, energy transfer in buildings, and electronic equipment cooling. The goal of this study is to investigate the effect of adding Al_2O_3 nanoparticles on the flow and heat characteristics of the low-pressure slip gaseous airflow in a square cavity in which the hot wall is attached to two fins. Moreover, the effect of the Knudsen number (Kn), the Rayleigh number (Ra) and volume fraction of the nanoparticles on these characteristics will be addressed and discussed thoroughly.

A low-pressure flow is classified based on (Kn). Referring to Schaaf and Chambre **[1]**; Cercignani and Lampis **[2]**, four different flow regimes are identified: continuum regime, slip regime, transitional regime, and free molecular regime. For slip flows, both slip velocity and temperature jump boundary conditions are applied at the surfaces.

Due to the importance of natural convection in cavities, extensive studies have been conducted, both experimentally and numerically. For instance, Bilgen **[3]** studied the natural convection heat transfer in differentially heated cavities numerically. In his study, streamlines and isotherms are produced, and effects of the Rayleigh number and the relative conductivity ratio on the flow characteristics is carried out. The results show that the Nusselt number increases as the Rayleigh number increases and the Nusselt number decreases as the relative conductivity ratio increases. Alkhalidi et al. **[4]** investigated the buoyancy-driven heat transfer in rarefied gas inside a conjugate cavity. The governing equations along with the slip flow and temperature jump boundary conditions are solved using a finite-volume technique. Simulations are carried out for different conductivity ratios, Rayleigh numbers, and cavity tilt angles. Moreover, a correlation among the Nusselt number and those parameters is proposed. In their study, Benseghir and Rahal **[5]** carried out a numerical simulation of heat transfer in a square cavity with two fins attached to

*Corr. Author's Address: 1German Jordanian University, Mechatronics Engineering Department, Jordan, wael.alkouz@gju.edu.jo

the hot wall. A parametric study is presented for the Rayleigh number equalling 10^5 and different dimensionless positions of the fin. They determined that there is an optimum position of the fins to achieve the maximum heat transfer. In their work, Al-Kouz et al. [6] numerically investigated low-pressure flow and heat transfer characteristics in an inclined enclosed cavity in which the hot wall is attached to two fins, the effects of the Knudsen number, the Rayleigh number, porosity of the fins, location of the fins, length of the fins, tilt angle and the conductivity ratio are presented. In addition, a correlation of the Nusselt number among these parameters is proposed. In the reviewed work conducted by Öztop et al. [7], two- and three-dimensional numerical investigations along with experimental techniques are used to investigate the effects of the type and location of the heat source on the flow and heat characteristics of the flow inside enclosed cavities. Furthermore, the effects of different boundary conditions and different configurations on the flow and heat characteristics inside enclosed cavities are identified and reported.

Enhancement of heat transfer by utilizing nanofluid has attracted great attention and motivated the investigation of such flows in recent decades. This is mainly due to their relevance to many engineering applications, such as those found in automotive cooling industry. Due to the increasing need for ultrahigh performance cooling systems, nanofluids have been recently investigated as next-generation coolants for car radiators as stated by Bigdeli et al. [8]. Furthermore, nanofluids can be found in the electronic cooling industry and many others.

Akbari et al. [9] studied forced the turbulent convection of Al_2O_3-water and Cu-water inside horizontal tubes. They showed that dispersing the nanosolid particles in the flow improves thermophysical and thus enhances heat transfer. However, some penalties are paid due to the increase in pressure drop. Balandin et al. [10] reported that by adding graphene to the base fluid, the resulting thermal conductivity will enhance heat transfer.

Experimental and numerical works have revealed many different types of nanoparticles that have been used to enhance the heat transfer; these include but are not limited to metals and oxide metals. In this research, we will consider adding Al_2O_3 to the base fluid (low-pressure air) in a square cavity in which the hot wall is attached to two fins.

The type and concentration of the nanoparticles affect the thermal behaviour of the resulting nanofluid. Many research studies, both numerical and experimental have tackled this issue such as Akbari et al. [9], Balandin et al. [10], Kalteh et al. [11], and Hussein et al. [12].

Excellent reviews of the heat transfer characteristics of nanofluid in forced and free convection flows can be found in the studies of Wang and Mujumdar [13], Yu et al. [14], Sarkar et al. [15], Saidur et al. [16], Suresh et al. [17] and Hussien et al. [12].

A state-of-the-art review of the viscosity of nanofluid is given in Murshed and Estellé [18], in which different models available in the literature along with their application range are reported. Also, effects of temperature and the concentration of the nanoparticles on the heat transfer characteristics have been identified and explicitly reviewed.

Dispersing Al_2O_3 in the base fluid is a common practice in many thermal applications. Adding these particles will enhance the thermal conductivity of the resulting fluid.

Labib et al. [19] computationally investigated the effect of base fluid on convective heat transfer utilizing Al_2O_3 nanoparticles. Their results show that ethylene-glycol-base fluid will give better heat transfer enhancement than that of water.

Experimental investigation of convective heat transfer of Al_2O_3 water nanofluid in circular tubes has been studied by Heris et al. [20], Nusselt numbers of nanofluids were obtained for different nanoparticle concentrations as well as for different Reynold and Peclet numbers. Experimental results show that mixing the base fluid with nanoparticles is superior to the single base fluid as far as the heat transfer enhancement is concerned. In the work presented by Moghadassi et al. [21], CFD modelling of a horizontal circular tube was utilized to study the effect of nanofluids on laminar forced convective heat transfer. In their study, water-based Al_2O_3 and Al_2O_3-Cu hybrid nanofluids were considered. The results show that the hybrid nanofluid resulted in a higher convective heat transfer coefficient. Experimental results illustrated by Noie et al. [22] show that suspended nanoparticles (Al_2O_3) in water nanofluid enhanced the heat transfer in a two-phase closed thermosyphon; different volume fractions were taken into consideration. In their work, results show that the efficiency of the two-phase closed thermosyphon increases up to (14.7 %) when adding Al_2O_3 nanoparticles to the base fluid.

Salman et al. [23] solved numerically laminar convective heat transfer in a two-dimensional microtube with constant heat flux. They considered different types of nanofluids with different nanoparticle sizes and different volume fractions. They found that the Nusselt number increases

with the volume fraction and decreases with the nanoparticle size. Moreover, the Nusselt number increases with the Reynolds Number. Williams et al. [24] investigated the turbulent convective heat transfer and pressure loss of aluminium water nanofluid in horizontal tubes; different particle concentrations were considered. They compared their results with the available traditional single-phase correlations for fully developed flow; no abnormal heat transfer enhancement was observed in the study. Steady laminar mixed convection flow in a lid-driven square cavity filled with Al_2O_3 water nanofluid was investigated computationally by Taamneh and Bataineh [25]. Different volume fractions of the nanoparticles as well as different Richardson numbers were considered. Simulation results show that adding nanoparticles to the base fluid will increase the heat transfer rate. In addition, increasing the Richardson number increases the average Nusselt number.

Although there are many research studies that deal with the heat transfer characteristics, there is a lack of studies that consider the heat transfer characteristics of low-pressure gaseous nanofluids. In this paper, further insight on adding nanoparticles to the low-pressure gaseous flow and heat transfer characteristics in the square cavity of length L in which two solid fins are attached to the hot wall is provided. In the present study, $0 \leq \phi \leq 0.2$, $0 \leq Kn \leq 0.1$ to cover both continuum and slip flow regimes. $10^3 \leq Ra \leq 10^6$ to study the effect of both conduction dominant versus convection dominant modes of heat transfer. L_F/L is set to 0.5 m; H_F takes the value of 0.25 to 0.75. A finite volume numerical computational fluid dynamics (CFD) solution utilizing the Boussinesq approximation is used to obtain the solution for such flows. The Prandtl number (Pr) is taken to be constant and is equal to 0.7. The Knudsen number was varied by controlling the pressure inside the cavity. The effects of Kn, Ra, and the nanoparticles' volume fraction on the flow and heat transfer characteristics are investigated.

1 MATHEMATICAL FORMULATION

1.1 Governing Equations

In this study, two-dimensional laminar and steady-state natural convection flow is investigated. The Boussinesq approximation is utilized to account for the buoyancy force, and all other fluid properties are considered constant. Fig. 1 represents flow in the geometry under investigation, which is a square cavity of length L in which two fins are attached to the hot wall. In this study, continuum and slip flow regimes are considered.

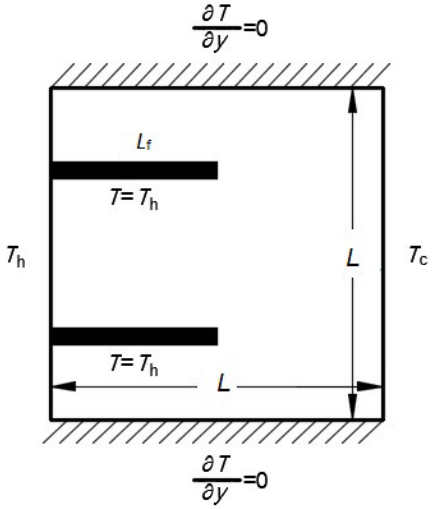

Fig. 1. *The geometry used for the computational domain*

Adding nanoparticles to the base fluid will change the thermophysical properties of the resulting nanofluid. It is assumed that the suspension of the nanoparticles is homogeneous with well-dispersed nanoparticles (i.e. no particle aggregation). Following Hussien et al. [12] and Cardellini et al. [26], the properties of the nanofluid can be calculated based on the following equations:

Viscosity:

We adapted the Brinkman model [27] for viscosity since the range of the volume fraction of the nanosolid particles investigated is below 0.2. It is also important to mention here that we had examined the results from another viscosity model, of Hatschek [28] for $\phi = 0.2$ and the difference between the Brinkman model and Hatcheck model is less than 1% for $\phi = 0.2$.

The Brinkman model for viscosity is as follows:

$$\mu_{nf} = \frac{\mu_f}{(1-\varphi)^{2.5}}. \tag{1}$$

Density:

$$\rho_{nf} = (1-\varphi)\rho_f + \varphi\rho_s. \tag{2}$$

Heat capacitance:

$$Cp_{nf} = (1-\varphi)(Cp)_f + \varphi(Cp)_s. \tag{3}$$

Thermal expansion coefficient:

$$\beta_{nf} = \beta_f \left[\frac{1}{1+\frac{(1-\varphi)\rho_f}{\varphi\rho_s}} \frac{\beta s}{\beta_f} + \frac{1}{1+\frac{\varphi\rho_s}{1-\varphi\rho_f}} \right]. \quad (4)$$

Thermal conductivity:

Following the Maxwell-Garnett (MG) **[29]** model and based on the assumption that the suspension is homogeneous with well-dispersed nanoparticles, then:

$$k_{nf} = k_f \frac{k_s + 2k_f - 2\varphi(k_f - k_s)}{k_s + 2k_f + \varphi(k_f - k_s)}. \quad (5)$$

Table 1 summarizes the thermophysical properties used to obtain the resulting properties of the Al_2O_3-air nanofluid.

Table 1. *Thermophysical properties for air and Al_2O_3*

Physical properties	Air	Al_2O_3
C_p [J/(kg K)]	1006.43	765
ρ [kg/m^3]	1	3970
k [W/m^{2}K]	0.025	40
β [1/K]	0.00333	0.0000085
α [m^2/s]	0.000019	0.00001317

To calculate the resulting properties of the nanofluid, user-defined functions (UDFs) were used in Fluent 18. The governing equations that describe the problem under investigation are summarized below:

Continuity:

$$\frac{\partial u}{\partial x} + \frac{\partial v}{\partial y} = 0. \quad (6)$$

x- momentum:

$$\rho_{nf}\left(u\frac{\partial u}{\partial x} + v\frac{\partial u}{\partial y} \right) = -\frac{\partial P}{\partial x} + \mu_{nf}\left[\frac{\partial^2 u}{\partial x^2} + \frac{\partial^2 u}{\partial y^2} \right]. \quad (7)$$

y- momentum:

$$\rho_{nf}\left(u\frac{\partial v}{\partial x} + v\frac{\partial v}{\partial y} \right) = -\frac{\partial P}{\partial y} - \rho_{nf} g + \mu_{nf}\left[\frac{\partial^2 v}{\partial x^2} + \frac{\partial^2 v}{\partial y^2} \right]. \quad (8)$$

Energy:

$$\rho_{nf} C_{pnf}\left(u\frac{\partial T}{\partial x} + v\frac{\partial T}{\partial y} \right) = k_{nf}\left[\frac{\partial^2 T}{\partial x^2} + \frac{\partial^2 T}{\partial y^2} \right]. \quad (9)$$

The boundary conditions applied for the slip flow regime are the temperature jump and slip velocity at the hot and cold walls of the cavity; reported by Karniadakis et al. **[30]**, Lockerby et al. **[31]** and Kandlikar et al. **[32]** as follows:

$$u_w - u_g = \left(\frac{2-\sigma_v}{\sigma_v} \right) \lambda \frac{\partial u}{\partial n} \approx \left(\frac{2-\sigma_v}{\sigma_v} \right) Kn\left(u_g - u_c \right), \quad (10)$$

$$v_g = 0, \quad (11)$$

$$T_w - T_g = \left(\frac{2-\sigma_T}{\sigma_T} \right) \frac{2\gamma}{\gamma+1} \frac{k}{\mu c_v} \lambda \frac{\partial T}{\partial n} \approx \approx \left(\frac{2-\sigma_T}{\sigma_T} \right) \frac{2\gamma}{\gamma+1} \frac{k}{\mu c_v} K_n \left(T_g - T_c \right), \quad (12)$$

where σ_v and σ_T represent the momentum and thermal accommodation coefficients.

The corresponding Knudsen number is defined as follows:

$$Kn = \frac{\lambda}{L}, \quad (13)$$

where λ is the mean free path, and L is the length of the square cavity.

Thermal boundary conditions are imposed at $x=0$ and L such that:

At $(x = 0, y)$, $T = T_h$, (14)

At $(x = L, y)$, $T = T_c$,, (15)

where T_h is the hot surface temperature, and T_c is the cold surface temperature, the fins' temperature is set to T_h.

The local heat flux is calculated as follows:

$$q''_F = -k\frac{\partial T}{\partial n}\Big|_F, \quad (16)$$

$$q''_h = -k\frac{\partial T}{\partial n}\Big|_h, q''_c = -k\frac{\partial T}{\partial n}\Big|_c. \quad (17)$$

Heat transfer from the hot to the cold wall is calculated by integrating the local heat flux along the wall of the hot wall and the fins as follows:

$$Q = \sum \left(\int_{A_h} q''_h dA_h + \int_{A_F} q''_F dA_F \right) = \int_{A_c} q''_c dA_c. \quad (18)$$

Then, the average heat transfer coefficient along the wall of the hot surface and the fin or along the wall of the cold surface is calculated by combining Eqs. (16) to (18).

$$\bar{h} = \frac{Q}{(T_i - T_\circ)A_T} = \frac{Q}{(T_i - T_\circ)A_c}. \quad (19)$$

From Eq. (19), the average Nusselt number can be calculated as follows based on the unit length of the cavity:

$$Nu = \frac{\bar{h}L}{k_{nf}} = \frac{\bar{h}}{k_{nf}}. \quad (20)$$

2 NUMERICAL SOLUTION

In this study, a finite volume analysis is used to serve as a method of solution for the problem under investigation. Initially, a mesh of 40×40 elements is tested. The SIMPLE algorithm, reported by Versteeg and Malalasekera **[33]** and Patankar and Spalding **[34]**, is used. In addition, the PRESTO algorithm is utilized to calculate the pressure field. To differentiate the convective terms, a hybrid second order accuracy scheme of central and upwind difference is used. All momentum and thermal accommodation coefficients are assumed to be unified for all simulations. It is worth mentioning here that the effect of the momentum and thermal accommodation coefficients on the Nusselt number has been examined; it was found that the Nusselt number is insensitive to these coefficients in comparison to the rest of the parameters considered in this study. Table 2 illustrates the effects of momentum and thermal accommodation coefficients on the Nusselt number for the case in which $Ra = 10^6$, $\phi = 0.02$ and $Kn = 0.05$, the table shows that these coefficients have almost negligible effects on the Nusselt number. The solution is considered to be converged when the maximum of the normalized absolute residual across all nodes is less than 10^{-6}.

Table 2. *Effects of the momentum and thermal accommodation coefficients on the Nusselt number for the case in which Ra = 10⁶, ϕ = 0.02 and Kn = 0.05*

σ_v	σ_T	*Nu*
0	0	1.9582
0.05	0.05	1.9586
1	1	1.9588

3 GRID INDEPENDENCE

The grid that was used in all simulations is illustrated in Fig. 2. It consists of a two-dimensional mesh. As a starting mesh, the grid step sizes are increasing in the x and y directions with expansion factors of 1.06 and 1.15, respectively; these values were chosen in order to capture the gradients' near solid-fluid interface. Then the mesh was adapted in which velocity gradients near the solid surfaces are calculated. More cells were added to reduce the gradients below a certain value. It was observed that any further change in these parameters would not affect the results. A grid sensitivity analysis test is carried out by monitoring the average Nusselt number at the cold wall, and solutions were obtained for different numbers of grid nodes. It was obvious that adding more cells beyond a certain value will not change the value of the average Nusselt number at the cold surface of the square cavity.

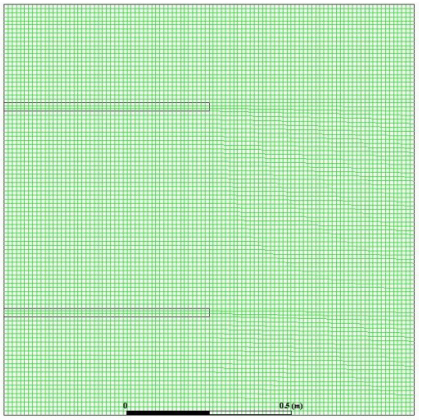

Fig. 2. *Adaptive grid system technique used in the simulations*

Fig. 3 demonstrates that the solution is mesh-independent for a grid of 100×100 nodes. This grid size is used for all simulations conducted in this research.

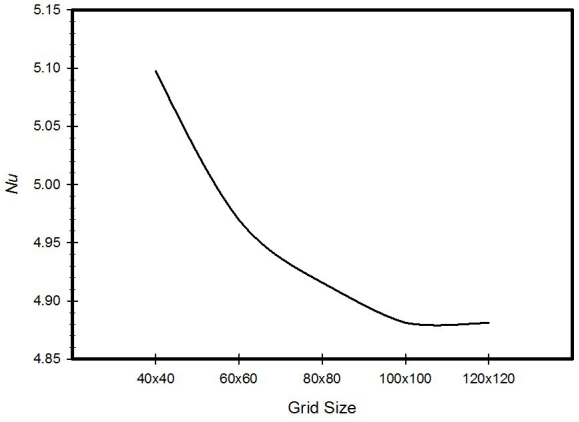

Fig. 3. Grid independence test

4 CODE VERIFICATION

To verify the numerical code, the results of the current code are compared with the results obtained by De Vahl Davis and Jones **[35]**, De Vahl Davis **[36]**

and Sarkar et al. [37] for the case of gaseous airflow inside a square cavity with no fins attached to the hot wall. Table 3 shows a comparison between the mean Nusselt number at the cold surface obtained by the current code and that obtained by [34] to [36] at Ra = 10^4, 10^5 and 10^6. Comparisons show excellent agreement with an error of less than 1 %. In addition, Fig. 4 shows results from the current code compared to the results obtained by Taamneh and Bataineh [25] at ϕ = 0.01 and different Richardson numbers (Ri) for the case of mixed convection heat transfer in a square-lid-driven cavity filled with water/Al_2O_3 nanofluid. The figure illustrates that there is a maximum error of 3 %.

Table 3. *Comparison between results obtained from present study and those obtained by* [34] *to* [36]

Ra	10^4	10^5	10^6
[35], [36]	2.243	4.519	8.800
[37]	2.24	4.51	8.82
Present study	2.241	4.52	8.83

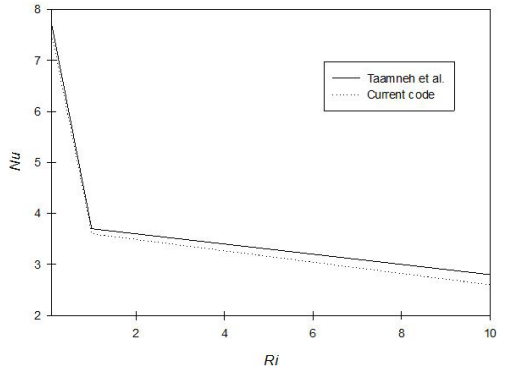

Fig. 4. *Comparison between results obtained from the current code to results obtained by Taamneh and Bataineh* [25]

5 RESULTS AND DISCUSSION

Fig. 5 shows the velocity stream function contours inside the square cavities with a fin position of H_F = 0.25 to 0.75 and fin lengths of 0.5 m for the cases with Knudsen number values of zero, 0.01, 0.05 and 0.1 to cover the continuum and slip flow regimes. Moreover, two different values of the nanoparticles volume fraction of ϕ=0.01 and 0.2 are also considered. The streamlines are plotted for cases where Ra=10^5. By inspecting the streamlines, it is obvious from the graphs that a large clockwise rotating cell is formed. By increasing the Knudsen number by the same volume fraction, less circulation is observed inside the cavity in the regions between the two fins, between the upper fin and the upper wall, and between the lower fin and the lower wall. This decrease in circulation and distortion of the streamlines will affect the heat transfer characteristics as will be shown later. The hot fluid near the hot wall (left wall) is rising and replacing the cold fluid near the cold wall (right wall) that is falling. For the cases of ϕ=0.2 and different Knudsen numbers, it is clear that more changes to the flow are observed (more recirculating regions) in comparison to ϕ=0.01. Greater recirculation in the flow and distorted streamlines will lead to better heat transfer enhancement.

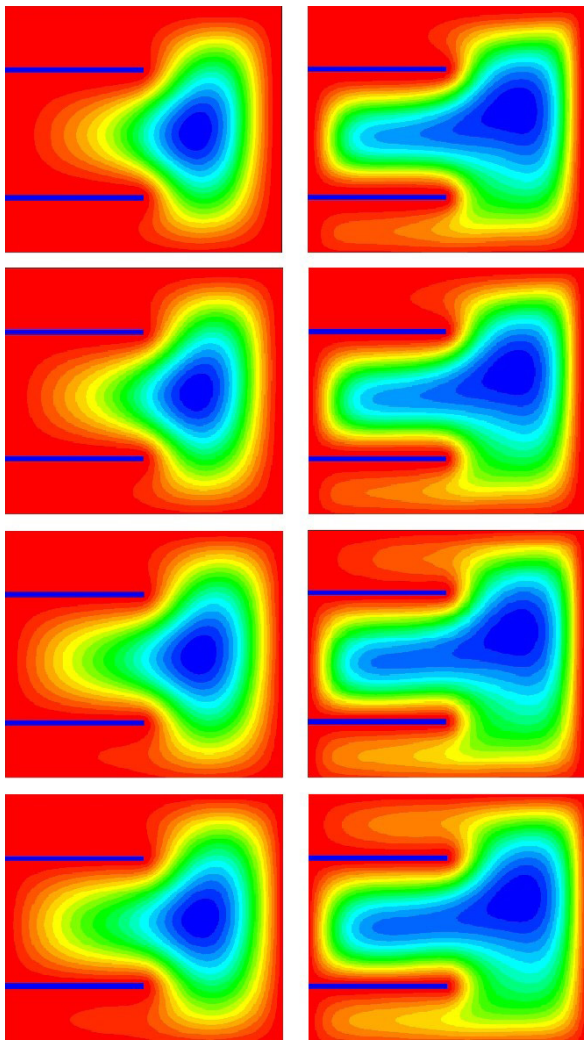

Fig. 5. Streamlines, Kn = 0, 0.01, 0.05, 0.1 at two different nanoparticle volume fractions (ϕ=0.01 and 0.2)

Fig. 6 shows the isothermal contours inside the square cavities for the same cases and parameter values considered in Fig. 4. By observing the contours for the case of ϕ=0.01 and different Knudsen numbers. It is

found that for the case of higher Knudsen numbers, mostly the area near the fins are affected while the rest of the cavity is almost unaffected; for the case of the Knudsen number equalling zero, more area inside the cavity is affected and more distortion of the contours occurred. For the case of $\phi = 0.2$, remarkable distortion and recirculation in the flow are happening compared to the cases of $\phi = 0.01$. It is also obvious that by increasing the Knudsen number, less distortion, mixing and recirculation of the flow are happening. This will affect the heat transfer characteristics.

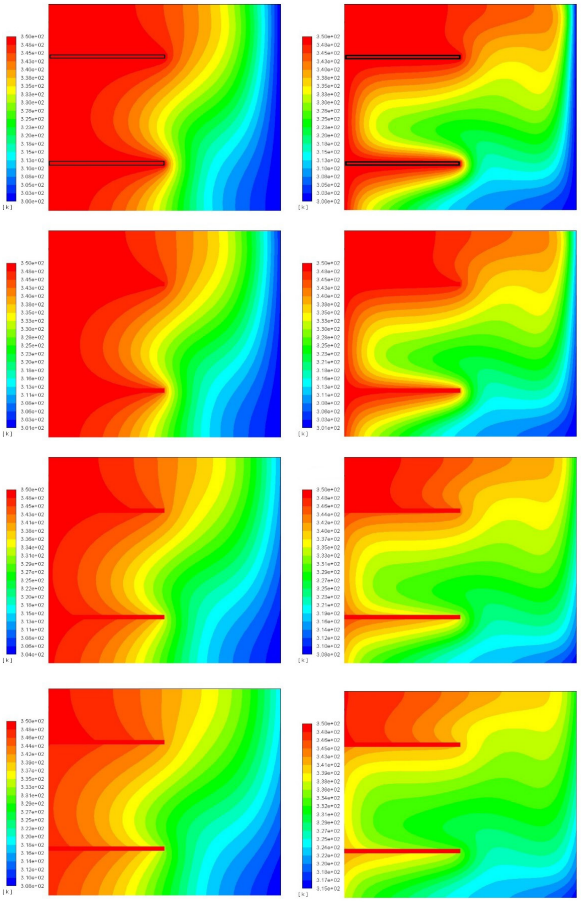

Fig. 6. *Isotherms, Kn = 0, 0.01, 0.05, 0.1 at two different nanoparticle volume fractions ($\phi = 0.01$ and 0.2)*

Fig. 7 illustrates the variation in the vertical velocity V_y along the horizontal centreline of the cavity with the length of the cavity (L), in which the Knudsen number takes the value of 0.05 and different values of Rayleigh numbers. The graph shows that as that Rayleigh number increases the vertical velocity near the walls will increase; this will enhance the heat transfer. It is worth mentioning here that in the region away from the walls; the vertical velocity is almost constant, which means that the dominant mode of heat transfer in this region is conduction, while at the walls it is convection. For low values of Rayleigh number, the figure indicates that there is no variation of the vertical velocity, and the dominant mode of heat transfer is condution.

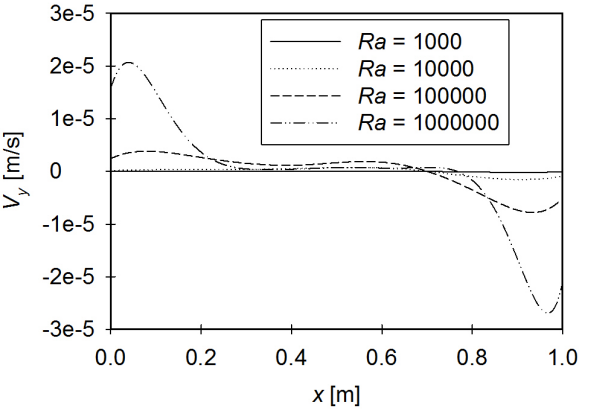

Fig. 7. *Variation of the vertical velocity (V_y) with the length of the cavity (L) for different Rayleigh numbers, Kn = 0.05*

In Fig. 8, the temperature distributions T along the horizontal centreline of the cavity are plotted against the length of the cavity (L) for different Rayleigh numbers at a fixed value of the Knudsen number of 0.05. The graph shows that as the Rayleigh number increases, the convection heat transfer becomes the dominant mode of heat transfer, this is very clear from the variation of the temperature at the wall boundaries for higher Rayleigh numbers. For the cases of lower values of Rayleigh numbers, the conduction mode of heat transfer dominates.

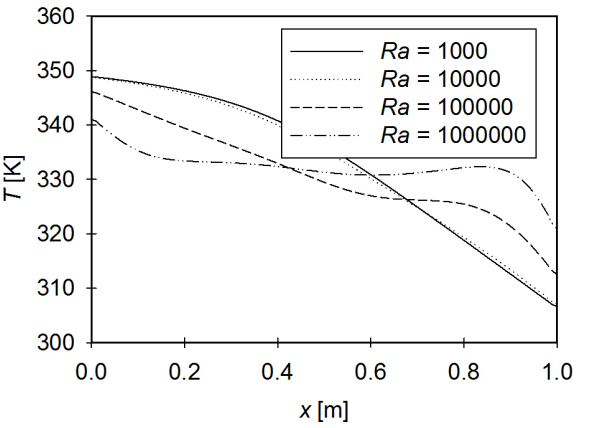

Fig. 8. *Variation of the temperature (T) with the length of the cavity (L) for different Rayleigh numbers, Kn = 0.05*

Vertical velocity (V_y) variations along the centreline of the cavity at constant Rayleigh number

of 10^6 and different Knudsen numbers that cover the continuum and slip regimes are plotted in Fig. 9. The graph shows that as the Knudsen number increases then the slip velocity at the boundaries will increase; this will result in less heat transfer and, consequently, a lower Nusselt number.

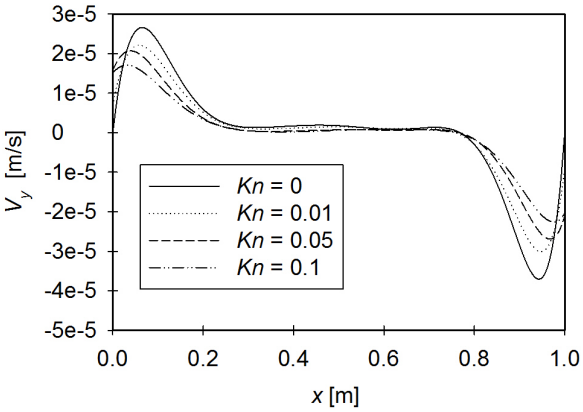

Fig. 9. *Variation of the vertical velocity (V_y) with the length of the cavity (L) for different Knudsen numbers, Ra = 10^5*

Fig. 10 demonstrates the temperature variations along the centreline of the cavity at $Ra = 10^6$ and different values of Knudsen numbers that cover the continuum and slip flow regimes. The graph shows that as the Knudsen number increases, the temperature jump at the hot wall increases.

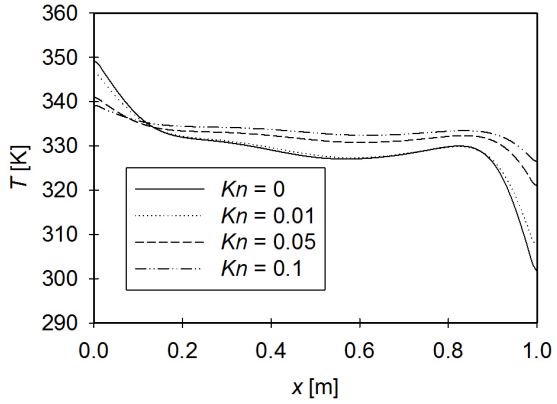

Fig. 10. *Variation of the temperature (T) with the length of the cavity (L) for different Knudsen numbers, Ra = 10^5*

Variations of the Nusselt number with Rayleigh number at different volume fractions and $Kn = 0.1$ are plotted in Fig. 11. The graph shows that the Nusselt number increases as the Rayleigh number increases for all values of the volume fractions considered in this study. Moreover, the graph shows that the Nusselt number increases as the volume fraction increases for the same value of the Rayleigh number. The graph also shows that when the Rayleigh number is below 10^4, the dominant mode of heat transfer is conduction. In addition, when $10^4 < Ra < 10^5$ then there is a combination of conduction and convection modes of heat transfer happening inside the cavity while for the range where Ra is greater than 10^5, the dominant mode of heat transfer is mainly convection.

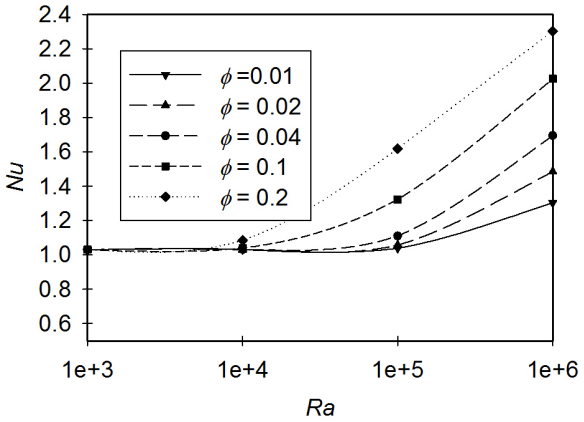

Fig. 11. *Variation of Nusselt number (Nu) with the Rayleigh number (Ra) at different ϕ, Kn = 0.1*

In Fig. 12, variations of the Nusselt number with the solid nanoparticles volume fraction (ϕ) for different values of the Knudsen number and $Ra = 10^6$ are plotted. The graph shows that as ϕ increases the Nusselt number increases for all values of the Knudsen number. For instance, and at $Kn = 0.05$, the graph shows that there is a percentage increase of 53 % in the Nusselt number for the case when $\phi = 0.2$ compared to $\phi = 0.01$. Moreover, the graph shows that as the Knudsen number increases the Nusselt number decreases. This can be justified due to the rarefaction effects.

Finally, a correlation for the Nusselt number among all the parameters taken into consideration in this study in the slip flow regime and $\phi \neq 0$ is proposed in the following equation with $R^2 = 0.87$:

$$Nu = 0.2196 Ra^{0.0829} Kn^{-0.511} \varphi^{0.104} . \quad (21)$$

It should be noted that the range of Rayleigh numbers used in the simulation is the reason for the weak dependency of Nusselt numbers on Rayleigh numbers. Rayleigh number range is from the conduction dominant heat transfer all the way to the transitional regime between the conduction and convection heat transfer.

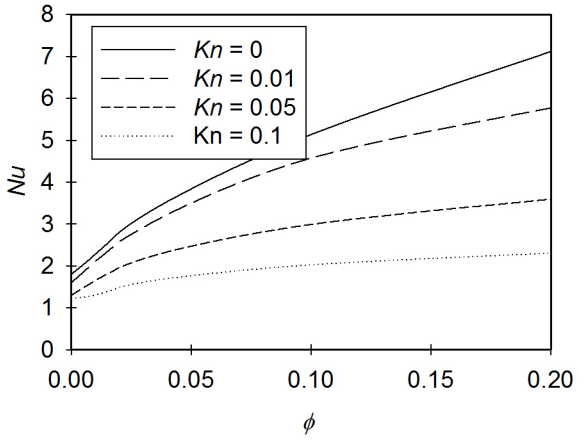

Fig. 12. *Variation of Nusselt number (Nu) with the volume fraction (ϕ) at different Kn*

Based on Eq. (21), one can plot many master curves to show the effects of the investigated parameters on the Nusselt number. For instance, Fig. 13 shows one master curve in which *Ra* is fixed to 10^6, and the Knudsen number and the nanoparticles volume fraction were varied. Many other similar curves can also be generated.

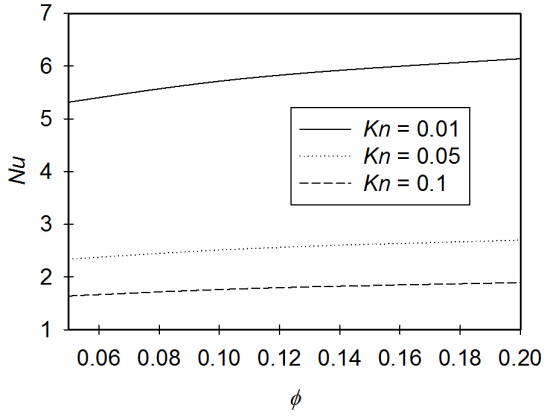

Fig. 13. *Variation of Nusselt number (Nu) with the volume fraction (ϕ) at different Kn for the case where Ra = 10^6 and based on Eq. (21)*

6 CONCLUSIONS

A steady, two-dimensional analysis of low-pressure gaseous laminar nanofluid flow inside a square cavity in which the hot surface is attached to two solid fins is carried out. This type of flow serves in many engineering applications such as those in nuclear reactors and electronic equipment cooling. Rarefaction, Rayleigh numbers, and the volume fraction of the nanoparticles effects on both flow and heat characteristics of such flows are investigated. Results show that as the Knudsen number increases, the slip velocity and the temperature jump at the boundaries will increase and the average Nusselt number decreases. Moreover, it is found that as the Rayleigh number increases, the Nusselt number increases. In addition, it is found for the investigated range of the nanoparticles volume fraction that as this fraction increases then the average Nusselt number increases. Finally, a correlation among the Nusselt number and the parameters investigated in this study is proposed.

7 NOMENCLATURE

A_c Cold wall area, [m^2]
A_h Hot wall area, [m^2]
A_F Fin area, [m^2]
A_T Area of the fin and the hot wall $A_T = A_h + A_F$, [m^2]
C_p Specific heat, [J kg^{-1} K^{-1}]
g Gravity acceleration in the x direction, [m·s^{-2}]
Gr Grashof number, [-]
h_1 Fin 1 Position, [m]
h_2 Fin 2 Position, [m]
h Convection heat transfer coefficient, [W m^{-2} K^{-1}]
k Thermal conductivity, [W m^{-1} K^{-1}]
Kn Knudsen number, [-]
k_f Fluid thermal conductivity, [W m^{-1} K^{-1}]
k_{nf} Nanofluid thermal conductivity, [W m^{-1} K^{-1}]
k_s Nano particles thermal conductivity, [W m^{-1} K^{-1}]
L Length of the square cavity, [m]
L_F Fin length, [m]
Nu Nusselt number, [-]
P Pressure, [Pa]
Q Heat transfer, [W]
q''_c Local heat flux at the wall of the cold surface, [W·m^{-2}]
q''_h Local heat flux at the wall of the hot surface, [W·m^{-2}]
q''_F Local heat flux at the fin, [W·m^{-2}]
R Universal gas constant, [J·mol^{-1}·K^{-1}]
Ra Rayleigh number, [-]
Re Reynolds number, [-]
Ri Richardson number (Gr/Re^2)
T Temperature, [°C]
T_c Temperature of the first cell from the wall, [°C]
T_i Hot surface temperature, [°C]
T_o Cold surface temperature, [°C]
u Velocity in x-direction, [m·s^{-1}]
u_c Tangential velocity of the first cell from the wall, [m·s^{-1}]
v Velocity in y-direction, [m·s^{-1}]
x, y Cartesian coordinates, [m]

Greek symbols

α Thermal diffusivity [$m^2 \cdot s^{-1}$]
β Thermal expansion coefficient, [K^{-1}]
γ Specific weight, [$N \cdot m^{-3}$]
λ Molecular mean free path, [m]
μ Dynamic viscosity, [$kg\ m^{-1}\ s^{-1}$]
v Kinematic viscosity, [$m^2 \cdot s^{-1}$]
ϕ Nano particles volume fraction, [%]
P Density of air, given by ideal gas equation (P/RT), [$kg \cdot m^{-3}$]
σ_T Thermal accommodation coefficient
σ_v Momentum accommodation coefficient

Subscripts

eff Effective
f Fluid
F Fin
g Gas flow
i Hot wall
n Normal
nf Nanofluid
o Cold wall
r Ratio
w wall

8 REFERENCES

[1] Chambre, A.P., Schaaf, S.A., (1961). *Flow of Rarefied Gases*, Princeton University Press Princeton, **DOI:10.1515/9781400885800**.

[2] Cercignani, C., Lampis, M. (1974). Half space models for gas-surface interaction. *Rarefied Gas Dynamics*, Academic Press, New York, p. 361-368, **DOI:10.1016/B978-0-12-398150-9.50040-7.**

[3] Bilgen, E. (2005). Natural convection in cavities with a thin fin on the hot wall. *International Journal of Heat and Mass Transfer*, vol. 48, no. 17, p. 3493-3505, **DOI:10.1016/j.ijheatmasstransfer.2005.03.016**.

[4] Alkhalidi, A., Kiwan, S., Al-Kouz, W., Alshare, A. (2016). Conjugate heat transfer in rarefied gas in enclosed cavities. *Vacuum*, vol. 130, p. 137-145, **DOI:10.1016/j.vacuum.2016.05.013**.

[5] Chahrazed, B., Samir, R. (2012). Simulation of heat transfer in a square cavity with two fins attached to the hot wall. *Energy Procedia*, vol. 18, p. 1299-1306, **DOI:10.1016/j.egypro.2012.05.147**.

[6] Al-Kouz, W., Kiwan, S., Alshare, A., Alkhalidi, A., Al-Muhtady, A., Saadeh, H. (2017). Two dimensional analysis of low-pressure flows in an inclined square cavity with two fins attached to the hot wall, in press, *International Journal of Thermal Sciences*.

[7] Öztop, H.F., Estellé, P., Yan, WM.., Al-Salem, K., Orfi, J., Mahian, O. (2015). A brief review of natural convection in enclosures under localized heating with and without nanofluids. *International Communications in Heat and Mass Transfer*, vol. 60, p. 37-44, **DOI:10.1016/j.icheatmasstransfer.2014.11.001**.

[8] Bigdeli, M.B., Fasano, M., Cardellini, A., Chiavazzo, E., Asinari, P. (2016). A review on the heat and mass transfer phenomena in nanofluid coolants with special focus on automotive applications. *Renewable and Sustainable Energy Reviews*, vol. 60, no. 1615-1633, **DOI:10.1016/j.rser.2016.03.027**.

[9] Akbari, M., Galanis, N., Behzadmehr, A. (2012). Comparative assessment of single and two-phase models for numerical studies of nanofluid turbulent forced convection. *International Journal of Heat and Fluid Flow*, vol. 37, p. 136-146, **DOI:10.1016/j.ijheatfluidflow.2012.05.005**.

[10] Balandin, A.A., Ghosh, S., Bao, W., Calizo, I., Teweldebrhan, D., Miao, F., Lau,C.N. (2008). Superior thermal conductivity of single-layer graphene. *Nano Letters*, vol. 8, no. 3, 902-907, **DOI:10.1021/nl0731872**.

[11] Kalteh, M., Abbassi, A., Saffar-Avval, M., Frijns, A., Darhuber, A., Harting, J. (2012). Experimental and numerical investigation of nanofluid forced convection inside a wide microchannel heat sink. *Applied Thermal Engineering*, vol. 36, p. 260-268, **DOI:10.1016/j.applthermaleng.2011.10.023**.

[12] Hussien, A.A., Abdullah, M.Z., Al-Nimr, M.A. (2016). Single-phase heat transfer enhancement in micro/minichannels using nanofluids: Theory and applications. *Applied Energy*, vol. 164, p. 733-755, **DOI:10.1016/j.apenergy.2015.11.099**.

[13] Wang, X.-Q., Mujumdar, A.S. (2007). Heat transfer characteristics of nanofluids: a review. *International Journal of Thermal Sciences*, vol. 46, no. 1, p. 1-19, **DOI:10.1016/j.ijthermalsci.2006.06.010**.

[14] Yu, W., France, D.M., Routbort, J.L., Choi, S.U.S. (2008). Review and comparison of nanofluid thermal conductivity and heat transfer enhancements. *Heat Transfer Engineering*, vol. 29, no. 5, p. 432-460, **DOI:10.1080/01457630701850851**.

[15] Sarkar, J., Ghosh, P., Adil, A. (2015). A review on hybrid nanofluids: Recent research, development and applications. *Renewable and Sustainable Energy Reviews*, vol. 43, p. 164-177, **DOI:10.1016/j.rser.2014.11.023**.

[16] Saidur, R., Leong, K.Y., Mohammad, H.A. (2011). A review on applications and challenges of nanofluids. *Renewable and Sustainable Energy Reviews*, vol. 15, no. 3, p. 1646-1668, **DOI:10.1016/j.rser.2010.11.035**.

[17] Suresh, S., Venkitaraj, K.P., Selvakumar, P., Chandrasekar, M. (2012). Effect of Al2O3–Cu/water hybrid nanofluid in heat transfer. *Experimental Thermal and Fluid Science*, vol. 38, p. 54-60, **DOI:10.1016/j.expthermflusci.2011.11.007**.

[18] Murshed, S.M.S., Estellé, P. (2017). A state of the art review on viscosity of nanofluids. *Renewable and Sustainable Energy Reviews*, vol. 76, p. 1134-1152, **DOI:10.1016/j.rser.2017.03.113**.

[19] Labib, M.N., Nine, Md.J., Afrianto, H., Chung, H., Jeong, H. (2013). Numerical investigation on effect of base fluids and hybrid nanofluid in forced convective heat transfer. *International Journal of Thermal Sciences*, vol. 71, p. 163-171, **DOI:10.1016/j.ijthermalsci.2013.04.003**.

[20] Heris, S.Z., Esfahany, M.N., Etemad, S.Gh. (2007). Experimental investigation of convective heat transfer of Al2O3/water nanofluid in circular tube. *International Journal of Heat and Fluid Flow*, vol. 28, no. 2, p. 203-210, **DOI:10.1016/j.ijheatfluidflow.2006.05.001**.

[21] Moghadassi, A., Ghomi, E., Parvizian, F. (2015). A numerical study of water based Al2O3 and Al2O3–Cu hybrid nanofluid effect on forced convective heat transfer. *International Journal of Thermal Sciences*, vol. 92, p. 50-57, **DOI:10.1016/j.ijthermalsci.2015.01.025**.

[22] Noie, S.H., Heris, S.Z., Kahani, M., Nowee, S.M. (2009). Heat transfer enhancement using Al2O3/water nanofluid in a two-phase closed thermosiphon. *International Journal of Heat and Fluid Flow*, vol. 30, no. 4, p. 700-705, **DOI:10.1016/j.ijheatfluidflow.2009.03.001**.

[23] Salman, B.H., Mohammed, H.A., Kherbeet, A.Sh. (2012). Heat transfer enhancement of nanofluids flow in microtube with constant heat flux. *International Communications in Heat and Mass Transfer*, vol. 39, no. 8, p. 1195-1204, **DOI:10.1016/j.icheatmasstransfer.2012.07.005**.

[24] Williams, W., Buongiorno, J., Hu, L.-W. (2008). Experimental investigation of turbulent convective heat transfer and pressure loss of alumina/water and zirconia/water nanoparticle colloids (nanofluids) in horizontal tubes. *Journal of Heat Transfer*, vol. 130, no. 4, p. 042214, **DOI:10.1115/1.2818775**.

[25] Taamneh, Y., Bataineh, K. (2017). Mixed convection heat transfer in a square lid-driven cavity filled with Al2O3-water nanofluid. *Strojniški vestnik - Journal of Mechanical Engineering*, vol. 63, no. 6, 383-393, **DOI:10.5545/sv-jme.2017.4449**.

[26] Cardellini, A., Fasano, M., Bigdeli, M.B., Chiavazzo, E., Asinari, P. (2016). Thermal transport phenomena in nanoparticle suspensions. *Journal of Physics: Condensed Matter*, vol. 28, no 48, p. 1-17, **DOI:10.1088/0953-8984/28/48/483003**.

[27] Brinkman, H.C. (1952). The viscosity of concentrated suspensions and solutions. *The Journal of Chemical Physics*, vol. 20, no. 4, p. 571-581, **DOI:10.1063/1.1700493**.

[28] Hatschek, E. (1913). The general theory of viscosity of two phase systems. *Transactions of the Faraday Society*, vol. 9, p. 80-92, **DOI:10.1039/TF9130900080**.

[29] Maxwell, J.C. (1873). *A Treatise on Electricity and Magnetism*, vol. 1. Clarendon Press, Oxford.

[30] Karniadakis, G., Beskok A., Aluru, N. (2005). *Microflows and Nanoflows*, Springer, New York.

[31] Lockerby, D.A., Reese, J.M., Emerson, D.R., Barber, R.W. (2004). Velocity boundary condition at solid wall in rarefied gas calculations. *Physical Review E*, vol. 70, no. 1, p. 017303, **DOI:10.1103/PhysRevE.70.017303**.

[32] Kandlikar, S., Garimella, S., Li, D., Colin, S., King, M. R. (2006). *Heat Transfer and Fluid Flow in Minichannels and microchannels: Single-Phase Gas Flow in Microchannels*, Elsevier Ltd.

[33] Versteeg, H.K., Malalasekera, W. (1995). *An Introduction to Computational Fluid Dynamics: The Finite Volume Method*, Prentice-Hall, Essex.

[34] Patankar, S.V., Spalding, D.B. (1972). A calculation procedure for heat, mass and momentum transfer in three-dimensional parabolic flows. *International Journal of Heat and Mass Transfer*, vo. 15, no. 10, p. 1787-1806, **DOI:10.1016/0017-9310(72)90054-3**.

[35] De Vahl Davis, G. , Jones, I.P. (1983). Natural convection in a square cavity: A comparison exercise. *International Journal of Numerical Methods in Fluids*, vol. 3, no. 3, p. 227-248, **DOI:10.1002/fld.1650030304**.

[36] De Vahl Davis, G. (1983). Natural convection of air in a square cavity: A bench mark numerical solution. *International Journal of Numerical Methods in Fluids*, vol. 3, no. 3, p. 249-264, **DOI:10.1002/fld.1650030305**.

[37] Sarkar, A., Nag, A., Sastri, V.M.K. (1993). Natural convection in a differentially heated square cavity with a horizontal partition plate on the hot wall. *Computer Methods in Applied Mechanics and Engineering*, vol. 110, no. 1-2, p. 143-156, **DOI:10.1016/0045-7825(93)90025-S**.